


Onset of Rotational Decoupling for a Molecular Ion Solvated in Helium: From Tags to Rings and Shells

Julia A. Davies¹, Christoph Schran^{2,*†}, Fabien Briec^{2,‡}, Dominik Marx², and Andrew M. Ellis^{1,§}
¹*School of Chemistry, University of Leicester, University Road, Leicester, LE1 7RH, United Kingdom*
²*Lehrstuhl für Theoretische Chemie, Ruhr-Universität Bochum, 44780 Bochum, Germany*

 (Received 21 July 2022; revised 5 December 2022; accepted 18 January 2023; published 24 February 2023)

Little is known about how rotating molecular ions interact with multiple ^4He atoms and how this relates to microscopic superfluidity. Here, we use infrared spectroscopy to investigate $^4\text{He}_N \cdots \text{H}_3\text{O}^+$ complexes and find that H_3O^+ undergoes dramatic changes in rotational behavior as ^4He atoms are added. We present evidence of clear rotational decoupling of the ion core from the surrounding helium for $N > 3$, with sudden changes in rotational constants at $N = 6$ and 12. In sharp contrast to studies on small neutral molecules microsolvated in helium, accompanying path integral simulations show that an incipient superfluid effect is not needed to account for these findings.

DOI: [10.1103/PhysRevLett.130.083001](https://doi.org/10.1103/PhysRevLett.130.083001)

The superfluid response of bulk liquid helium is a many-body quantum effect derived from bosonic exchange of ^4He atoms at very low temperature [1]. However, it is less clear if and when a small cluster of helium atoms can become a superfluid. A way of exploring this is through systematic variation of the number of helium atoms attached to a molecule, where the spectroscopy of that molecule is used to probe the surrounding helium. Experiments with a number of small linear molecules, such as OCS [2,3], CO [4], N_2O [5], and CO_2 [6] have shown a decrease in the rotational constant of the molecule as the first few helium atoms are added, as expected classically given the increase in moment of inertia of the resulting complex. However, the addition of further helium atoms reverses that behavior and the molecular rotation begins to decouple from the surrounding helium. This reduction in rotational “friction” has been attributed to a nanoscale version of the famous Andronikashvili experiment [7], suggesting that a superfluid response can begin with relatively few helium atoms (between 6 and 10) [2–6].

Interpretation of this incipient superfluid effect has come from path integral Monte Carlo and other quantum simulations [8–18]. Put simply, the first few helium atoms do not allow any meaningful bosonic exchange, and thus adiabatically follow the rotation of the molecule, decreasing the rotational constant. However, as more helium atoms are added, longer permutation cycles involving multiple helium atoms become accessible. It is these permutation cycles that are connected to the superfluid response [10,19], and this mechanism is now widely accepted as the explanation for the decoupling of molecular rotation from the surrounding helium.

Even though 20 years have passed since the first experimental study of the rotational decoupling of helium

from a small and neutral molecule as the number of ^4He atoms is increased in a stepwise manner [2], no equivalent experimental studies for charged molecules have been reported. Although molecular cations with a single attached helium atom have been well studied [20], the addition of multiple helium atoms poses more of a challenge, not least because ion formation is an energetic process that is often incompatible with the low temperatures needed to attach multiple helium atoms. Cryogenic ion traps offer a potential route, as, for example, in rotationally resolved studies of $\text{He}_2 \cdots \text{CH}_3^+$ [21], and $\text{He}_{2,3}\text{H}^+$ [22], and a recent mass spectrometry study of $\text{He}_{1-5} \cdots \text{H}_3\text{O}^+$ [23]. At the other extreme, spectroscopic investigations of molecular ions fully solvated inside liquid helium nanodroplets containing thousands of atoms are also possible [24–26].

Given the absence of information on how an ion transitions to the fully solvated limit upon the stepwise addition of helium, we address this here by forming ion-helium complexes via electron ionization of superfluid helium nanodroplets doped with neutral molecules [27]. The resulting mass-selected molecular ion-helium complexes are then probed using infrared (IR) photodissociation spectroscopy [28–30]. Because of the mass selectivity that is readily afforded for ions, spectral congestion from different sized complexes is not an issue and so, when it comes to investigating rotational behavior, we are no longer limited to the small linear molecules used in earlier studies on neutral species [2–6].

The ion chosen in the current study is the hydronium ion H_3O^+ . The spectroscopic technique has allowed IR spectra of the $^4\text{He}_N \cdots \text{H}_3\text{O}^+$ complexes to be recorded as a function of N with up to 15 helium atoms, exceeding the number required to form a complete and essentially spherical shell of helium density around the dopant (see

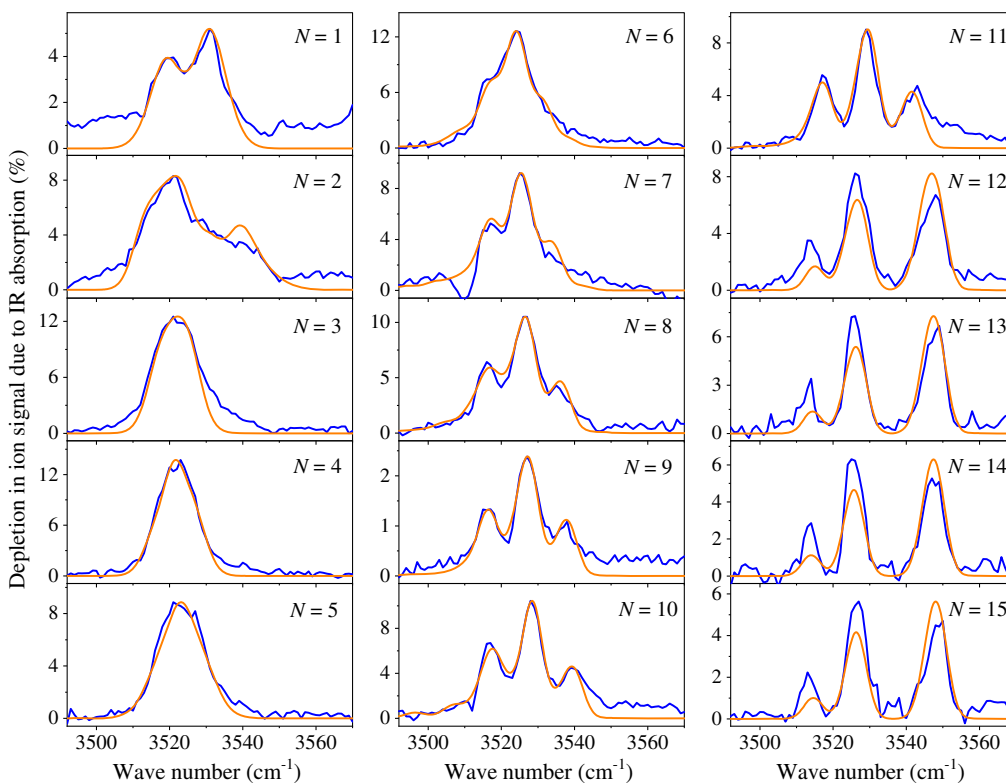


FIG. 1. Infrared spectra of $\text{He}_N \cdots \text{H}_3\text{O}^+$ for $N = 1$ to 15. Experimental spectra are represented by blue lines, while simulated spectra are shown in orange. The simulations for $N \leq 3$ use rotational constants from *ab initio* calculations, whereas for $N \geq 3$ the rotational constants have been varied for optimum agreement with experiment.

later). Notably, H_3O^+ has a substantially lower moment of inertia and greater binding energy to helium than dopants used in previous studies for such values of N . We relate these experimental measurements to accurate path integral quantum simulations, which are sensitive to temperature-dependent coupling of H_3O^+ with the helium environment, including the bosonic nature of ^4He . In marked contrast to past work, theory can account for the observations without invoking a microscopic superfluid effect.

Figure 1 shows experimental IR spectra measured in the OH stretching region of H_3O^+ for values of N from 1 to 15, inclusive. Rotational structure is partly resolved in some of the spectra and the variation with N is striking. Broad and structured spectral profiles are observed for $N = 1$ and 2, whereas a single Gaussian-like feature is seen for $N = 3, 4$, and 5. For $N = 6$ and 7, a pronounced shoulder appears to the red of the main peak, while asymmetry is observed to the blue. At $N = 8$ there are clear signs of rotational sidebands on each side of the most intense peak, and their relative separation gradually increases up to $N = 11$. This substructure can be accounted for by assuming a perpendicular vibrational transition within a (near) prolate symmetric top and $K = 1 \rightarrow 0, 0 \rightarrow 1$, and $1 \rightarrow 2$, transitions in order of increasing energy, where K is the quantum number for rotation about the axis of C_3 rotational symmetry in H_3O^+ . The observed increase in the

separation between these subbands indicates an increase in the rotational constant about the C_3 symmetry axis. Once $N = 12$ is reached, the spectrum undergoes a remarkable change in appearance, with a large separation of $>20 \text{ cm}^{-1}$ between the two dominant spectral peaks. This spectral profile is then retained up to the maximum value of N studied, which is 15. As we will show, the evolution of the rotational profiles reflects structural changes in the helium-ion complexes and a decoupling of the rotational motion of the ion from that of the surrounding helium.

To aid in the interpretation of the spectral profiles, the rotational structure has been simulated using the PGOPHER software package [31]. The results are included in Fig. 1, allowing a direct comparison with the experimental IR spectra. Table S1 in Supplemental Material [32] summarizes the quantities used in these simulations. Note that the global potential energy minimum structure for bare H_3O^+ has C_{3v} equilibrium symmetry. However, because this ion is known to undergo rapid (“umbrella”) inversion [33–37], it was necessary to use the D_{3h} molecular symmetry group in the rotational analysis (see Supplemental Material [32]) [38].

The spectral features shown in Fig. 1 derive from the excitation of antisymmetric OH stretching vibrations, which form a degenerate pair in bare H_3O^+ and have a far higher absorption cross section than the symmetric OH

stretch. The addition of a single helium atom to H_3O^+ leads to a structure in which the helium is bound to only one of the OH groups, forming a linear $\text{O}-\text{H}\cdots\text{He}$ moiety on average. This lowers the molecular symmetry, thus removing the vibrational degeneracy and thereby creating two vibrational bands with different frequencies. Only the lower frequency band, which has A_1 symmetry, falls within the frequency range shown in Fig. 1. For the $N = 2$ complex, the splitting between the two vibrational components is reduced, such that the two bands partially overlap. For $N = 3$, one helium atom is attached to each of the three OH groups on average, and so the original trigonal symmetry possessed by bare H_3O^+ returns for $\text{He}_3\cdots\text{H}_3\text{O}^+$, yielding a single vibrational band with E' symmetry.

In the simulations for $N \leq 3$, the rotational constants were taken from *ab initio* calculations (MP2/aug-cc-pVTZ), and the rotational temperature and vibrational frequency were then varied. Good agreement is seen with the rotational contours observed in the experimental spectra in Fig. 1. For complexes with $N \geq 4$, less rigid structures are expected because the additional atoms are located further from the areas of highest charge density within the H_3O^+ core. For such cases, the overall symmetry of the helium-ion complex is approximated to be that of the ion core and the rotational constants were systematically varied in the simulations, along with the rotational temperature and vibrational band origin, until good agreement was obtained with the experimental IR spectra. See Supplemental Material for further details [32].

The effect of adding helium atoms on the rotational behavior can be divided into its impact on (1) rotation about the C_3 symmetry axis of the bare H_3O^+ , which corresponds to the c inertial axis for $N \leq 3$ and the a inertial axis for $N \geq 4$, and (2) the overall tumbling rotation, which corresponds to the average rotation about the remaining axes. Starting with rotation about the C_3 axis, the rotational constant for $N = 1$ (0.61 cm^{-1}) is an order of magnitude lower than the value of $\sim 6.1\text{ cm}^{-1}$ for bare H_3O^+ (an oblate symmetric top) [33–35] because the $\text{He}\cdots\text{H}_3\text{O}^+$ complex rotates as a single rigid entity possessing an increased moment of inertia. The C_3 rotational constant declines further as more helium atoms are added and reaches a minimum at $N = 3$, as illustrated in Fig. 2(a). Thereafter, the rotational constant begins to increase, which we attribute to partial decoupling of the rotation of the ion core from the surrounding helium. A particularly large change, from 1.2 to 3.6 cm^{-1} , is observed between $N = 5$ and 6 , which is significant as it coincides with the completion of a ringlike helium structure that surrounds the H_3O^+ core [23]. When more than six helium atoms are added to H_3O^+ , the rotational constant continues to increase before reaching a plateau at 6.2 cm^{-1} (for $N \geq 12$). The similarity between the values for $N = 0$ and $N \geq 12$ suggests that rotation about the C_3 axis of symmetry is almost completely decoupled from the

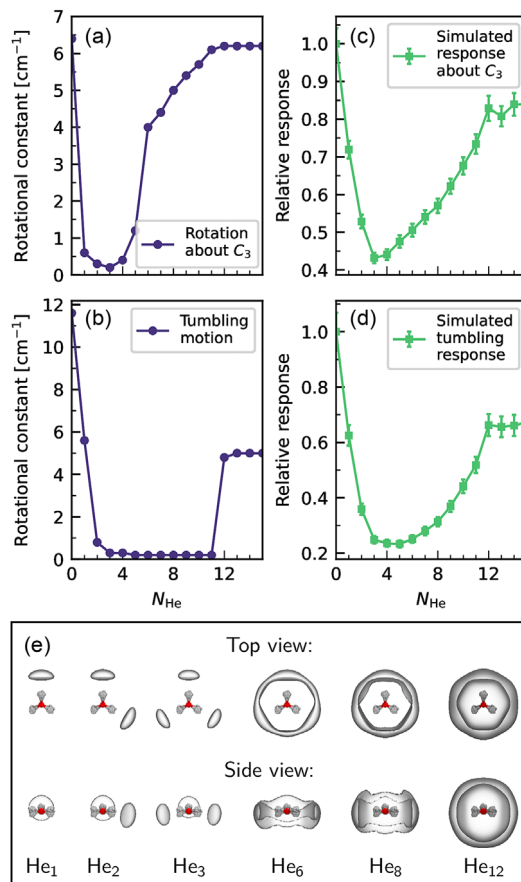


FIG. 2. N dependence of (a) the rotational constant about the C_3 axis of H_3O^+ and (b) the tumbling rotation of the H_3O^+ core, as determined from *ab initio* calculations for $N = 0$ to 3 and from analysis of the experimental data for $N = 4$ to 15 . The corresponding quantities obtained from PI simulations at 10 K are shown in (c) and (d). (e) Spatial distributions of helium around H_3O^+ for selected values of N from PI simulations.

surrounding helium at $N = 12$ (and beyond), which coincides with completion of a near-spherical solvation shell, as demonstrated in Fig. S6 in Supplemental Material [32].

The rotational constant associated with the tumbling motion also shows an initial rapid decline with N , as summarized in Fig. 2(b). It then remains small ($\leq 0.3\text{ cm}^{-1}$) between $N = 3$ and 11 , implying that the rotational motion stays strongly coupled to the helium. This is distinctly different from the partial decoupling observed at similar values of N for rotation about the C_3 axis. This unexpected result leads to rotational behavior replicating that of a prolate symmetric top for $N = 6$ – 11 , as opposed to an oblate top for the bare ion. A similar change in rotational behavior from oblate to prolate has previously been observed for CH_3^+ when fully solvated in helium nanodroplets [39]. In that case, it was attributed to the formation of a rigid $\text{He}_2-\text{CH}_3^+$ complex in which the two helium atoms lie along the C_3 axis, while the other helium atoms remain fluxional. In our case, it is assigned to differences in

the N -dependent decoupling of the rotational motion about the orthogonal molecular frame axes.

Figure 2(b) shows a profound change in the tumbling rotational constant, from 0.2 cm^{-1} for $N = 11$ to 4.5 cm^{-1} for $N = 12$. This indicates that this rotation suddenly becomes less hindered at $N = 12$, again coinciding with the near-spherical helium environment formed at this value of N . For $N \geq 12$, the rotational structure is largely unchanged and the tumbling constant levels off at $\sim 5.0\text{ cm}^{-1}$. This value is approximately half of that for the bare ion ($\sim 11.0\text{ cm}^{-1}$) [33–35], showing incomplete decoupling from the helium for this motion. As a result, the C_3 and tumbling rotational constants for $N \geq 12$ differ by only 20%. Hence, we have observed an N -dependent evolution in the overall rotational behavior from oblate to prolate to near-spherical top.

Path integral (PI) simulations were performed to provide atomistic insight into the ${}^4\text{He}_N \cdots \text{H}_3\text{O}^+$ complexes, while accounting for the fluxionality of the molecular ion and the bosonic quantum nature of the surrounding helium. The PI simulations used a hybrid PI molecular dynamics/PI Monte Carlo approach [40,41]. This allows us to rigorously include the rovibrational motion of nonrigid H_3O^+ , including its large-amplitude umbrella inversion, as well as its coupling to the helium environment, including bosonic exchange, within the ${}^4\text{He}_N \cdots \text{H}_3\text{O}^+$ complexes. In these simulations, the H_3O^+ potential energy surface and the $\text{He} \cdots \text{H}_3\text{O}^+$ interactions were described using neural network potentials [42,43] trained to reproduce highly accurate coupled cluster reference calculations [44,45] while the $\text{He} \cdots \text{He}$ interactions were described using a well-known pair potential [46]. This description of the potential energy surface is of the highest available accuracy, reproducing the “gold standard” in electronic structure theory, as given by basis set converged coupled cluster theory and benchmarked in detail in Supplemental Material [32].

The PI simulations provide insight into the helium solvation behavior, as well as the response of the H_3O^+ core. These show that the inversion motion of H_3O^+ is barely affected by the addition of helium atoms and so the ion will readily invert, exactly as assumed earlier when discussing the rotational structure simulations. Moreover, the PIMD/PIMC calculations reveal how the (micro) solvation structure changes as a function of the number of attached helium atoms. Of particular note is the formation of a helium torus in the H_3O^+ plane, which is continuous at $N = 5$ and is most pronounced for $N = 6$ [see Fig. 2(e)]. Thus, the strong decoupling of the rotation about the C_3 axis of H_3O^+ between $N = 5$ and $N = 6$ seen experimentally can be associated with this torus of helium density. As further helium atoms are added these locate above and below the torus until an almost spherical arrangement is reached at $N = 12$. This corresponds to the helium shell closing [see Fig. S5(a) in Supplemental Material [32]] and agrees well with the experimental observations.

To further explore the coupling of the rotation of H_3O^+ with the surrounding helium, we have analyzed imaginary time correlation functions using generalized coordinates that disentangle the rotation about the C_3 axis, the tumbling rotation, and the umbrella inversion. The strategy employed is similar to that reported elsewhere [47,48] and involves comparing the value of these correlation functions at imaginary time $\tau/2$ as a function of N to that of bare H_3O^+ . This makes it possible to obtain a qualitative picture of the responses for rotation about the C_3 axis of H_3O^+ and for the tumbling motion. We resort to this strategy due to the absence of exact quantum dynamics approaches at finite temperature that include bosonic exchange. The findings are shown in Figs. 2(c) and 2(d), alongside the corresponding experimental quantities. The agreement between theory and experiment is quite remarkable. In particular, for rotation about the C_3 axis, theory captures both the minimum at $N = 3$ and the asymptotic behavior for $N \geq 12$. The agreement for the tumbling motion is not quite as good, although the relatively minor change predicted from $N = 3$ to 8 is similar to experiment. The initial decline with N and the return to a plateau at $N = 12$ is also mirrored in the PIMD/PIMC simulations.

The observed rotational behavior, namely an initial decrease in rotational constant as helium atoms are added followed by an increase, is similar to that reported for small neutral linear molecules [2–6]. It is surprising to discover this behavior for a molecular ion H_3O^+ , given the much stronger interaction with helium expected for a small ion than would be the case for a neutral molecule. The key question to answer is the cause of this unexpected rotational decoupling. Does it result from an incipient superfluid response, as claimed in case of the neutral molecules? The PI data shown in Figs. 2(c) and 2(d) were calculated at a temperature of 10 K. At such a relatively high temperature, boson exchange, which is the underlying cause of superfluidity, should be insignificant, and this is confirmed by the very small superfluid fraction calculated [49] at this temperature (see Fig. S9 in Supplemental Material [32]). When the temperature is lowered to 1 K, boson exchange now occurs but the same calculated solvation structure and rotational responses are seen for $N = 1$ up to 12 as at 10 K, confirming that a microscopic superfluid effect is not responsible for the experimental observations.

If the rotational response is not caused by the onset of superfluidity, as reported previously for neutral molecules, then what else might be responsible? The most likely explanation stems from H_3O^+ being a relatively fast rotor. It is well known that fast rotors, molecules with large rotational constant(s) such as HF, CH_4 , and NH_3 , can rotate freely in liquid helium nanodroplets and have rotational constants similar to their gas phase values [50–52]. The current study shows that, despite the strong interaction of H_3O^+ with helium on account of the positive charge [44], rotational decoupling is possible with just a small number

of helium atoms. However, this decoupling only occurs once specific helium “structures” form. This first becomes possible when helium forms a torus around the molecular cation, coinciding with decoupling of the rotation about the C_3 axis of H_3O^+ and rotational behavior resembling that of a prolate symmetric top. Likewise, once helium forms a near-spherical distribution at $N = 12$, pronounced decoupling of the tumbling motion switches on.

Further experiments with dopants that are nonlinear, ionic and/or light rotors, may reveal whether H_3O^+ is unique in showing rotational decoupling that is independent of bosonic exchange. Alternative experimental techniques, such as rotational coherence spectroscopy, [53,54] may also provide valuable insight.

J. A. D. and A. M. E. thank the Leverhulme Trust for financial support (Grant No. RPG-2019-044), as well as the ALICE High Performance Computing Facility at the University of Leicester. D. M. was partially supported by Deutsche Forschungsgemeinschaft (DFG, German Research Foundation) via Grant No. MA 1547/19 and was also funded by DFG under Germany’s Excellence Strategy—EXC 2033–390677874—RESOLV. C. S. acknowledges partial financial support from the Alexander von Humboldt Foundation. The computational resources for the PI simulations were provided by HPC@ZEMOS, HPC-RESOLV, and BoViLab@RUB.

*Corresponding author (theoretical).
christoph.schran@rub.de

†Present address: Yusuf Hamied Department of Chemistry, University of Cambridge, Lensfield Road, Cambridge, CB2 1EW, United Kingdom.

‡Present address: Laboratoire Matière en Conditions Extrêmes, Université Paris-Saclay, CEA, DAM, DIF, 91297 Arpajon, France.

§Corresponding author (experimental).
andrew.ellis@le.ac.uk

- [1] P. Nozière and D. Pines, *Theory of Quantum Liquids, Volume II: Superfluid Bose Liquids* (Perseus, Boca Raton, 1999).
- [2] J. Tang, Y. Xu, A. R. W. McKellar, and W. Jäger, *Science* **297**, 2030 (2002).
- [3] A. R. W. McKellar, Y. Xu, and W. Jäger, *Phys. Rev. Lett.* **97**, 183401 (2006).
- [4] L. A. Surin, A. V. Potapov, B. S. Dumesh, S. Schlemmer, Y. Xu, P. L. Raston, and W. Jäger, *Phys. Rev. Lett.* **101**, 233401 (2008).
- [5] Y. Xu, W. Jäger, J. Tang, and A. R. W. McKellar, *Phys. Rev. Lett.* **91**, 163401 (2003).
- [6] J. Tang, A. R. W. McKellar, F. Mezzacapo, and S. Moroni, *Phys. Rev. Lett.* **92**, 145503 (2004).
- [7] E. L. Andronikashvili, *Zh. Eksp. Theor. Fiz.* **18**, 424 (1946).
- [8] Y. Kwon and K. B. Whaley, *Phys. Rev. Lett.* **83**, 4108 (1999).
- [9] Y. Kwon, P. Huang, M. V. Patel, D. Blume, and K. B. Whaley, *J. Chem. Phys.* **113**, 6469 (2000).
- [10] E. W. Draeger and D. M. Ceperley, *Phys. Rev. Lett.* **90**, 065301 (2003).
- [11] S. Moroni, A. Sarsa, S. Fantoni, K. E. Schmidt, and S. Baroni, *Phys. Rev. Lett.* **90**, 143401 (2003).
- [12] F. Paesani, A. Viel, F. A. Gianturco, and K. B. Whaley, *Phys. Rev. Lett.* **90**, 073401 (2003).
- [13] S. Moroni, N. Blinov, and P. N. Roy, *J. Chem. Phys.* **121**, 3577 (2004).
- [14] R. E. Zillich, Y. Kwon, and K. B. Whaley, *Phys. Rev. Lett.* **93**, 250401 (2004).
- [15] R. E. Zillich, Y. Kwon, and K. B. Whaley, *J. Chem. Phys.* **123**, 114301 (2005).
- [16] F. Paesani, Y. Kwon, and K. B. Whaley, *Phys. Rev. Lett.* **94**, 153401 (2005).
- [17] T. Zeng and P. N. Roy, *Rep. Prog. Phys.* **77**, 046601 (2014).
- [18] D. Mateo, F. Gonzalez, and J. Eloranta, *J. Phys. Chem. A* **119**, 2262 (2015).
- [19] W. Krauth, *Phys. Rev. Lett.* **77**, 3695 (1996).
- [20] E. J. Bieske and O. Dopfer, *Chem. Rev.* **100**, 3963 (2000).
- [21] M. Töpfer, P. C. Schmid, H. Kohguchi, K. M. T. Yamamda, S. Schlemmer, and O. Asvany, *Mol. Phys.* **117**, 1481 (2019).
- [22] M. Töpfer, A. Jensen, K. Nagamori, H. Kohguchi, T. Szidarovszky, A. G. Császár, S. Schlemmer, and O. Asvany, *Phys. Chem. Chem. Phys.* **22**, 22885 (2020).
- [23] D. Muller and O. Dopfer, *Phys. Chem. Chem. Phys.* **24**, 11222 (2022).
- [24] S. Smolarek, N. B. Brauer, W. J. Buma, and M. Drabbels, *J. Am. Chem. Soc.* **132**, 14086 (2010).
- [25] D. Verma, S. Erukala, and A. Vilesov, *J. Phys. Chem. A* **124**, 6207 (2020).
- [26] S. Erukala, A. Feinberg, A. Singh, and A. Vilesov, *J. Chem. Phys.* **155**, 084306 (2021).
- [27] M. Kuhn, M. Renzler, J. Postler, S. Ralser, S. Spieler, M. Simpson, H. Linnartz, A. G. G. M. Tielens, J. Cami, A. Mauracher, Y. Wang, M. Alcamí, F. Martin, M. K. Beyer, R. Wester, A. Lindinger, and P. Scheier, *Nat. Commun.* **7**, 13550 (2016).
- [28] J. A. Davies, N. A. Besley, S. Yang, and A. M. Ellis, *J. Phys. Chem. Lett.* **10**, 2108 (2019).
- [29] J. A. Davies, N. A. Besley, S. Yang, and A. M. Ellis, *J. Chem. Phys.* **151**, 194307 (2019).
- [30] J. A. Davies, S. Yang, and A. M. Ellis, *Phys. Chem. Chem. Phys.* **23**, 27449 (2021).
- [31] C. M. Western, *J. Quant. Spectrosc. Radiat. Transfer* **186**, 221 (2017).
- [32] See Supplemental Material at <http://link.aps.org/supplemental/10.1103/PhysRevLett.130.083001> for more details on the simulation of the rovibrational spectra and for full details of the path integral calculations.
- [33] M. H. Begemann and R. J. Saykally, *J. Chem. Phys.* **82**, 3570 (1985).
- [34] W. C. Ho, C. J. Pursell, and T. Oka, *J. Mol. Spectrosc.* **149**, 530 (1991).
- [35] J. Tang and T. Oka, *J. Mol. Spectrosc.* **196**, 120 (1999).
- [36] V. Špirko and W. P. Kraemer, *J. Mol. Spectrosc.* **134**, 72 (1989).
- [37] A. Miani, A. Beddoni, J. Pesonen, and L. Halonen, *Chem. Phys. Lett.* **363**, 52 (2002).
- [38] H. V. L. Nguyen, I. Gulaczyk, M. Kręglewski, and I. Kleiner, *Coord. Chem. Rev.* **436**, 213797 (2021).

- [39] S. Erukala, D. Verma, and A. Vilesov, *J. Phys. Chem. Lett.* **12**, 5105 (2021).
- [40] L. Walewski, H. Forbert, and D. Marx, *Comput. Phys. Commun.* **185**, 884 (2014).
- [41] F. Brieuç, C. Schran, F. Uhl, H. Forbert, and D. Marx, *J. Chem. Phys.* **152**, 210901 (2020).
- [42] J. Behler and M. Parrinello, *Phys. Rev. Lett.* **98**, 146401 (2007).
- [43] J. Behler, *Chem. Rev.* **121**, 10037 (2021).
- [44] C. Schran, F. Uhl, J. Behler, and D. Marx, *J. Chem. Phys.* **148**, 102310 (2018).
- [45] C. Schran, J. Behler, and D. Marx, *J. Chem. Theory Comput.* **16**, 88 (2020).
- [46] R. A. Aziz, A. R. Janzen, and M. R. Moldover, *Phys. Rev. Lett.* **74**, 1586 (1995).
- [47] A. Viel, K. B. Whaley, and R. J. Wheatley, *J. Chem. Phys.* **127**, 194303 (2007).
- [48] S. Miura, *J. Chem. Phys.* **126**, 114309 (2007).
- [49] P. Sindzingre, M. L. Klein, and D. M. Ceperley, *Phys. Rev. Lett.* **63**, 1601 (1989).
- [50] K. Nauta and R. E. Miller, *J. Chem. Phys.* **113**, 9466 (2000).
- [51] K. Nauta and R. E. Miller, *J. Chem. Phys.* **113**, 10158 (2000).
- [52] M. N. Slipchenko and A. F. Vilesov, *Chem. Phys. Lett.* **412**, 176 (2005).
- [53] B. Shepperson, A. A. Sondergaard, L. Christiansen, J. Kaczmarczyk, R. E. Zillich, M. Lemeshko, and H. Stapelfeldt, *Phys. Rev. Lett.* **118**, 203203 (2017).
- [54] A. S. Chatterley, L. Christiansen, C. A. Schouder, A. V. Jørgensen, B. Shepperson, I. N. Cherepanov, G. Bighin, R. E. Zillich, M. Lemeshko, and H. Stapelfeldt, *Phys. Rev. Lett.* **125**, 013001 (2020).